

Lowest-lying Tetra-Quark Hadrons in Anisotropic Lattice QCD

Mushtaq Loan^a, Zhi-Huan Luo^b, and Yu Yiu Lam^c

^a *International School, Jinan University, Huangpu Road West, Guangzhou 510632, P.R. China*

^b *Department of Applied Physics, South China Agricultural University, Wushan Road, Guangzhou, 510642, P.R. China*

^c *Department of Physics, Jinan University, Huangpu Road West, Guangzhou 510632, P.R. China*

(Dated: July 25, 2008)

We present a detailed study of lowest-lying $q^2\bar{q}^2$ hadrons in quenched improved anisotropic lattice QCD. Using the $\pi\pi$ and diquark-antidiquark local and smeared operators, we attempt to isolate the signal for $I(J^P) = 0(0^+), 2(0^+)$ and $1(1^+)$ states in two flavour QCD. In the chiral limit of light-quark mass region, the lowest scalar $4q$ state is found to have a mass, $m_{4q}^{I=0} = 927(12)$ MeV, which is slightly lower than the experimentally observed $f_0(980)$. The results from our variational analysis do not indicate a signature of a tetraquark resonance in $I = 1$ and $I = 2$ channels. After the chiral extrapolation the lowest $1(1^+)$ state is found to have a mass, $m_{4q}^{I=1} = 1358(28)$ MeV. We analysed the static $4q$ potential extracted from a tetraquark Wilson loop and illustrated the behaviour of the $4q$ state as a bound state, unbinding at some critical diquark separation. From our analysis we conclude that scalar $4q$ system appears as a two-pion scattering state and that there is no spatially-localised $4q$ state in the light-quark mass region.

PACS numbers: 11.15.Ha, 12.38.Gc, 11.15.Me

I. INTRODUCTION

The concept of multi-quark states has received revived interest due to the narrow resonances in the spectrum of states. The recent experimental observation of several new particles as candidates of multi-quark hadrons are expected to reveal new aspects of hadron physics [1, 2, 3, 4]. Among these discoveries, the tetraquark systems are also interesting in terms of their rich phenomenology, in particular the scalar mesons which still remain a most fascinating subject of research. The five 0^{++} isoscalar mesons below 2GeV: $f_0(400 - 1200)$, $f_0(980)$, $f_0(1370)$, $f_0(1500)$ and $f_0(1760)$ are subject of conflicting interpretations. $f_0(1370)$ is assigned to be lowest $q\bar{q}$ meson, $f_0(1500)$ and $f_0(1760)$ are expected to be the lowest scalar glueball or an $s\bar{s}$ scalar meson. The differences in the interpretations manifest themselves in the flavour wave functions of scalar-isoscalar mesons. To resolve the interpretational differences would require a detailed analysis of J/ψ decays into vector plus scalar mesons and the radiative decays like $f_0 \rightarrow \gamma\omega$ and $f_0 \rightarrow \gamma\phi$ that constrains the flavour structure. Such experiments are feasible at BESII [5, 6, 7, 8] and BESIII with good chances for all the channels in radiative J/ψ decays. The tetraquark systems are also interesting in terms of the nearly stable scalar charm state $D_0^*(1980)$, the narrow $D_0^*(2450)$, the analogue of $a_0(980)$ with open charm, $X(3872)$ and $Y(4260)$ [9, 10, 11, 12, 13]. From the consideration of their masses, narrow decay width and decay pattern, these states cannot be regarded as the simple mesons of $c\bar{c}$ or $c\bar{s}$ but conjectured to be $4q$ or molecular states [14, 15, 16].

While a phenomenological model may often be helpful in obtaining a qualitative understanding of the data, lattice QCD, at the present status of approximations, seems to provide a trustworthy guide into unknown territory in multi-quark hadron physics [17, 18]. It is expected

to play an important role in revealing the real nature of multi-quark hadrons. There are several, mainly exploratory, lattice studies of tetraquark systems available [19, 20, 21, 22, 23, 24, 25, 26], with mixed results. Most of these calculations claim the existence of a bound scalar $I = 0$ tetraquark state whereas Ref. [26] has observed no evidence for a $4q$ resonance. One may naively interpret the negative results obtained in Ref. [26] as a consequence of their combined analysis of maximum entropy method with hybrid boundary condition method on their choice of operators, which would strongly couple to two-pion scattering states. Thus, it is important to use various interpolating operators and variational techniques on more accumulated data to make a precise prediction. Our approach will be to use a number of different interpolating fields and smeared operators to enhance the low-lying spectra.

In this study, we provide a detailed analysis on tetraquark hadrons from the combination analysis of variational method and smearing on various interpolating fields on improved anisotropic lattices. Using the quenched approximation, and discarding quark-antiquark annihilation diagrams, we construct $q^2\bar{q}^2$ sources from multiple operators. We exclude the processes that mix $q\bar{q}$ and $q^2\bar{q}^2$ and allow the quark masses to vary from small to large values. In the absence of quark annihilation, we do not expect any mixing of $q^2\bar{q}^2$ with pure glue. Thus we can express the $q^2\bar{q}^2$ correlation functions in terms of a basis determined by gluon and quark exchange diagrams only. In the process of searching for a bound state it is essential to explore a large number of interpolating fields having the quantum numbers of the desired state. Explicitly, one needs to construct an interpolating field which has significant overlap with the $4q$ system. However, any $(qq\bar{q}\bar{q})$ operator must couple to hadronic states with the same quantum numbers (for example, the $\pi\pi$ scattering state). It is necessary to

disentangle the lowest-lying $4q$ states from the $\pi\pi$ scattering states, as well as the excited $4q$ states. To this end, we adopt a variational method to compute a $n \times n$ correlation matrix from the interpolating fields and from its eigenvalues we extract the masses.

The rest of the paper is organized as follows: in Sec. II, we discuss our choice of interpolating fields for the supposed scalar tetraquark state and outline our construction of the correlation matrix analysis. The technical details of the lattice simulations as well as the actions used in this study are discussed in Sec. III. It is essential to use the improved action that displays nearly perfect scaling, since large scaling violations could lead to a false signature of attraction. We therefore perform our simulations on improved lattice actions with tadpole-improved renormalised parameters that provide continuum limit results at finite-lattice spacing. We present and discuss our numerical results in Sec. IV. Finally, we perform the study of the inter-quark potential in our $4q$ system to establish a connection between connected $4q$ state and the ‘‘two-meson’’ state around the cross-over. Sec. V is devoted to our summary and concluding remarks.

II. LOWEST $q^2\bar{q}^2$ STATES ON THE LATTICE

We propose interpolators designed to maximize the possibility to observe attraction between tetraquark constituents at relatively heavy quark masses. Two general types of operators are considered: those based on the $\pi\pi$ configuration, and those based on a diquark-antidiquark configuration. The simplest $\pi\pi$ -type interpolators for the $I = 0$ and $I = 2$ channels, respectively, are

$$O_1^{I=0}(x) = \left[\left\{ (\bar{d}^a(x)\gamma_5 u^a(x)) (\bar{u}^b(x)\gamma_5 d^b(x)) \right. \right. \\ \left. \left. - (u \leftrightarrow d, \bar{u} \leftrightarrow \bar{d}) \right\} + \frac{1}{2} \left\{ (\bar{u}^a(x)\gamma_5 u^a(x)) \right. \right. \\ \left. \left. \times (\bar{d}^b(x)\gamma_5 d^b(x)) - (u \leftrightarrow d, \bar{u} \leftrightarrow \bar{d}) \right\} \right], \quad (1)$$

and

$$O_2^{I=2}(x) = (\bar{d}^a(x)\gamma_5 u^a(x)) (\bar{d}^b(x)\gamma_5 u^b(x)). \quad (2)$$

The $J^P = 1^+$ operator with isospin $I = 1$ is evaluated from the pseudo-scalar and vector mesons fields and has the form:

$$O_3^{I=1}(x) = \frac{1}{2} \left[(\bar{d}^a(x)\gamma_i u^a(x)) (\bar{d}^b(x)\gamma_5 u^b(x)) \right. \\ \left. - (\bar{d}^a(x)\gamma_5 u^a(x)) (\bar{d}^b(x)\gamma_i u^b(x)) \right. \\ \left. + (\bar{d}^a(x)\gamma_i u^a(x)) (\bar{d}^b(x)\gamma_i u^b(x)) \right]. \quad (3)$$

The other type of interpolating field is one in which quarks and antiquarks are coupled into a set of diquark and antidiquark, respectively and has the form

$$O_4(x) = \epsilon_{abc} [u_a^T C \Gamma d_b] \epsilon_{dec} [\bar{u}_d C \Gamma \bar{d}_e^T]. \quad (4)$$

Accounting for both colour and flavour antisymmetry, the possible Γ s are restricted to within γ_5 and γ_i . The

operators $O_{1,2}$ are similar to the naive pion \otimes pion operator with the difference that in the former one has a contribution from gluon and quark exchange diagrams to the $\pi - \pi$ four-point functions. The operator O_4 is motivated by the Jaffe-Wilzcek description of diquarks [27], which is expected to have a small overlap with two-meson scattering states.

A. Extraction of masses

The mass of the ground state is extracted from the asymptotic behaviour of the two-point the temporal $4Q$ correlator

$$C(t) = \frac{1}{V} \sum_{\vec{x}} \langle O(\vec{x}, t) O^\dagger(\vec{0}, 0) \rangle, \quad (5)$$

where the total momentum of the $4q$ system is projected to be zero. To disentangle the lowest-lying $4q$ states from $\pi\pi$ scattering states this way, we adopt a variational method to compute a 2×2 correlation matrix from two different interpolating fields.

We compute the propagators $\langle (O_i)_x (\bar{O}_j)_y \rangle$ with fixed $y = (\vec{0}, 0)$, and their time correlation functions,

$$C_{ij}(t) = \langle \sum_{\vec{x}} \text{tr} \left[\langle (O_i)(\vec{x}, t) \bar{O}_j(\vec{0}, 0) \rangle_f \right] \rangle_U, \quad (6)$$

where the trace sums over the Dirac space, and the subscripts f and U denote fermionic average and gauge field ensemble average, respectively. Following [17, 28, 29] we solve the eigenvalue equation

$$C(t_0) v_k(t_0) = \lambda_k(t_0) v_k(t_0) \quad (7)$$

to determine the eigenvectors $v_k(t_0)$ and use these eigenvectors to project the correlation matrices to the space corresponding to the n largest eigenvalues $\lambda_n(t_0)$

$$C_{ij}^n(t) = (v_i, C(t) v_j), \quad i, j = 1, \dots, n \quad (8)$$

and solve the generalised eigenvalue equation for the projected correlation matrix C_{ij}^n . In practice, we extract our results from a 2×2 correlation matrix. The masses are extracted from the average of C_{ij} by a single-exponential fit to $\lambda_i(t)$ for the range of t in which the effective mass

$$M_{eff} = \ln \left[\frac{\lambda(t)}{\lambda(t+1)} \right] \quad (9)$$

attains a plateau. However, to ensure the validity of our results, we compare them with those obtained using

$$M'_{eff} = \ln \left[\frac{\lambda(t-1) - \lambda(t)}{\lambda(t) - \lambda(t+1)} \right]. \quad (10)$$

B. Static $4q$ potential

The static tetraquark potential is extracted from the gauge invariant $4q$ Wilson loop. The $SU(3)$ Wilson loop is constructed by creating a $4q$ state at a time $t = 0$, which is annihilated at a later time t . Following [24, 25] we write the $4q$ Wilson loop as

$$W_{4q} = \frac{1}{12} \epsilon^{abc} \epsilon^{def} \epsilon^{a'b'c'} \epsilon^{d'e'f'} U(\mathbf{x}, \mathbf{x}', 1)^{aa'} U(\mathbf{x}, \mathbf{x}', 2)^{bb'} \\ \times U_G(\mathbf{x}, \mathbf{y})^{cf} U(\mathbf{y}', \mathbf{y}, 3)^{d'd} U(\mathbf{y}', \mathbf{y}, 4)^{e'e} \\ \times U_{G'}(\mathbf{y}', \mathbf{x}')^{f'c'} \quad (11)$$

where the staple-like links $U(\mathbf{x}, \mathbf{x}', k)$ are given by

$$U(\mathbf{x}, \mathbf{x}', k) = P \exp \left[ig \int_{\Gamma_k} dz^\mu A_\mu(z) \right],$$

where Γ_k denotes the path from \mathbf{x} to \mathbf{x}' for quark line k .

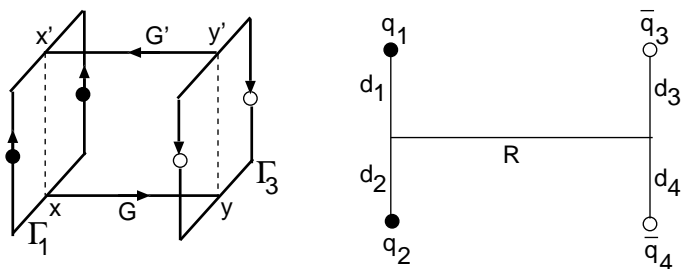


FIG. 1: The Wilson loop for the tetraquark system.

The junctions at \mathbf{x} and \mathbf{y} are joined by a line-like contour

$$U_G(\mathbf{x}, \mathbf{y}) = P \exp \left[ig \int_G dz \cdot \mathbf{A}(z) \right],$$

at $t = 0$. The tetraquark potential can be obtained from the large t behaviour of $\langle W_{4q} \rangle$, where the ground-state contribution becomes dominant. To obtain the optimal signal-to-noise ratio, we must suppress the contributions from the excited states, which may be done by APE smearing technique [30]. This involves replacing the space-like link variables U_i by smeared link variables. To tune the smearing parameters, we fix the smearing fraction to $\alpha = 0.7$, as it is sufficient to fix α and tune the smearing level to n_{APE} . A typical value which enhances the ground-state component in the $4q$ Wilson loop was $n_{APE} = 8$. The tetraquark potential is then extracted in the standard way from the large t behaviour of the $4q$ Wilson loop with a single-exponential fit:

$$\langle W_{4q} \rangle = Z e^{-V_{4q} t} \quad (12)$$

in the range $[t_{min}, t_{max}]$. The effective potential is then extracted from

$$V_{4q}(t) \equiv \ln \left[\frac{W_{4q}(t)}{W_{4q}(t+1)} \right]. \quad (13)$$

In this way, we calculate the potential for our planar $4q$ configurations.

III. SIMULATION DETAILS

To examine $q^2 \bar{q}^2$ in lattice QCD, we explore the improved actions on anisotropic lattices. With most of the finite-lattice spacing artifacts having been removed, one can use coarse lattices, with fewer sites and much less computational effort. It has been found that even on fairly coarse lattices these actions give good results for hadron masses by estimating the coefficients of the improvement terms using tadpole-improvement. Using a tadpole improved anisotropic gluon action [31], we generate quenched configurations on $16^3 \times 64$ lattice (with periodic boundary conditions in all directions) at $\beta = 4.0$. Gauge configurations are generated by a 5-hit pseudo heat bath update supplemented by four over-relaxation steps. These configurations are then fixed to the Coulomb gauge at every 500 sweeps. After discarding the initial sweeps, a total of 300 configurations are accumulated for measurements. Quark propagators are computed by using a tadpole-improved clover quark action on the anisotropic lattice [32]. All the coefficients in the action are evaluated from a tree-level tadpole improvement. We calculate the spectrum at quark masses as light as 0.004, which is much less than the hadronic scale, 1.0 GeV, associated with the scalar $4q$ system.

On each gauge fixed configuration, we invert the quark matrix by the BiCGstab algorithm to obtain the quark propagator. Using anti-periodic boundary conditions in the time direction, we calculate the propagators on three source time slices on the same lattice. For the lattice analysed here, we place the wall sources on the first, second and third time slices. Since there is a possibility of correlation among the propagators with different source time slices, we average them and treat them as a single result in a jackknife analysis.

The long distance exponential falloff is determined by the lowest-energy hadron state to which the operator couples. For lattice QCD, one has options to use a local or nonlocal interpolating operator for hadrons, provided its correlation function has a significant overlap with the state under consideration. To obtain a better overlap with the ground state, we used iterative smearing of gauge links and the application of the fuzzing technique for the fermion fields [33] taking the physical size of the particle into account. The fuzzed quark field is constructed to be symmetric in all space directions. Such a fuzzed quark field is only used at the sink, while the one at the source remains local. The application of fuzzing for two of the four quarks inside the $q^2 \bar{q}^2$ flattens the curvature of the effective mass. The largest plateau in the region with small errors is obtained with fuzzed u - and d -quarks. We used this variant to calculate our correlation functions.

We estimate the lattice spacing by linearly extrapolating the ρ mass to the physical quark mass. The latter can be determined from the ratio of two non-strange hadrons. Since m_u and m_d are fixed by the nucleon mass, in the non-strange sector, m_ρ is a test both for finite-size effects

and quenching errors. The major source of discrepancy among the lattice spacings from different observables is the quenching effect. The obtained ρ and N masses are compared to the experimental values and show a deviation of less than 3–4% for the lattice size explored here. Such a variance can be considered as the usual quenching effect. Inspired by the good agreement of the ρ and N masses with the experimental values, the scale was set alternatively by the ratio m_π/m_N . Using the experimental value 768 MeV for the rho mass, the spacing of our lattice is $a_s = 0.462(2)$ fm. The bare quark mass is determined by extracting the mass of the K meson. At $m_q a_t = 0.04$, we obtained the mass of vector meson $m_K = 553(2)$ MeV, which is in good agreement with the estimates obtained from other studies [28, 34]. Thus taking the strange quark bare mass to be $m_s a_t = 0.04$, we choose the bare quark masses for u and d to be much smaller than m_s , i.e., $m_q a_t = 0.01, 0.008, 0.0065, 0.0055, 0.005, 0.004$.

IV. RESULTS AND DISCUSSION

In this section we present the results of our lattice simulation of tetraquark masses for the isospin $I = 0, 1$ and $I = 2$ channels. In addition to extracting the masses of the $q^2\bar{q}^2$ states, we also study the mass differences between the candidate tetraquark states and the free two-particle states. This analysis is actually important in determining the nature of the states observed on the lattice, and the identification of the true resonances. Hence a lattice signature which might be observed for tetraquark resonance is a negative mass splitting at quark masses near the physical regime.

Fig. 2 shows the effective mass plot for the lowest scalar $4q$ ($ud\bar{u}\bar{d}$) for the typical hopping parameter $\kappa_t = 0.2635$. At sufficiently large t , contributions from excited states are diminished, and the correlator is dominated by a single state. Thus a plateau may serve as an indicator of the single-state saturation, hence allowing one to perform the single-exponential fit to the plateau region. In the region $0 \leq t \leq 9$, the effective mass for the $I = 0$ channel decreases monotonically and reaches a stable plateau at $10 \leq t \leq 25$. Beyond $t \sim 25$ the data become noisy. The fitting range $[t_{min}, t_{max}]$ for the final analysis is determined by fixing t_{max} and finding the range of t_{min} where the ground-state mass is stable against t_{min} . We choose one “best fit” which is insensitive to the fit range, has high confidence level and reasonable statistical errors. We then confirm this by looking at the plateau region of the correlator. Statistical errors of masses are estimated by the jackknife method. Since the analysed configurations were highly uncorrelated, which we ensured by separating the analysed configurations by as many as 1000 sweeps, the statistical errors of our mass estimates are typically on the few percent level. With most of our data we find that the errors are purely statistical, and the goodness of the fit is gauged by the χ^2/N_{DF} . All fits are reasonable, having

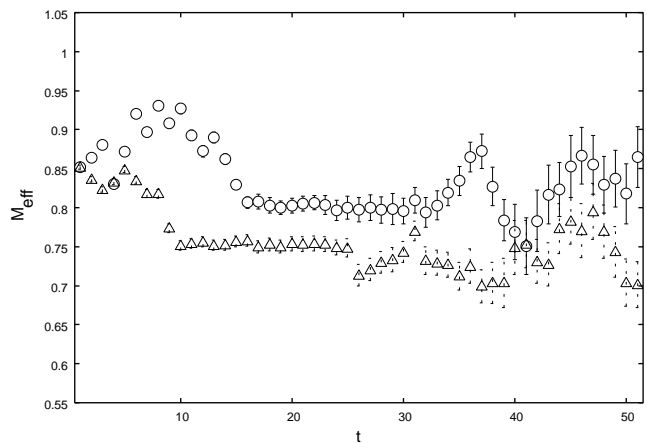


FIG. 2: Effective mass of $4q$ in the $I = 0$ (open triangles) and $I = 2$ (open circles) channels at $\kappa_t = 0.2635$ ($m_q a_t = 0.0065$).

$\chi^2/N_{DF} \leq 1$. For the $I = 2$ channel it was possible to find a fit region $[t_{15}, t_{35}]$ in which a convincing plateau was observed. The effective mass is found to be stable using different values of t in Eq. (9), which suggests that the tetraquark ground state is correctly projected.

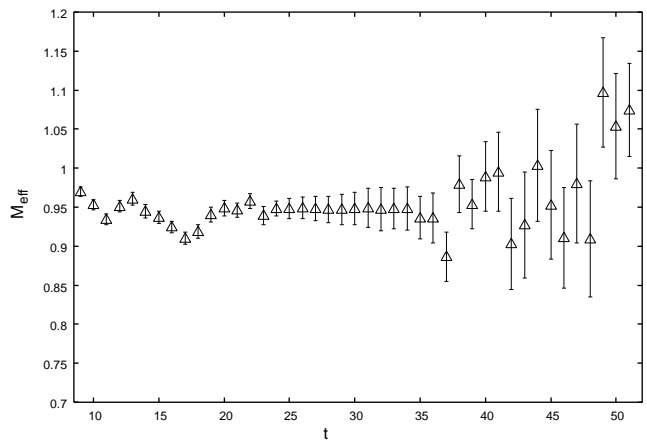


FIG. 3: Effective mass of $I(J^P) = 1(1^+) 4q$ state at $\kappa_t = 0.2650$ ($m_q a_t = 0.005$).

For the $I(J^P) = 1(1^+)$ tetraquark state, Fig. 3, we observe that the exponential seems to oscillate in time at the lowest-quark mass at large t . One can still demonstrate the existence of a plateau in the effective mass and extract the mass with some reliability, although the errors are relatively large. Suppressing any data point which has an error larger than its mean value, a possible plateau is seen in the region $20 \leq t \leq 35$ with reasonable errors, where the single-state dominance is expected to be achieved. To ensure the validity of our results, we compared them to those obtained using Eq. (10). It was found that the evaluations of (9) and (10) yield results very consistent within statistical errors.

The chiral extrapolation to the physical limit is the next important issue. From the view point of chiral per-

turbation theory, data points with smallest m_π^2 should be used to capture the chiral log behaviour. Leinweber et al. [35] demonstrated that the chiral extrapolation method based upon finite-range regulator leads to extremely accurate values for the mass of the physical nucleon with systematic errors of less than one percent. We use a set of data points with smallest m_π^2 to capture the chiral log behaviour. Fig. 4 collects and displays the resulting particle masses extrapolated to the physical quark mass value using linear and quadratic fits in m_π^2 ,

$$m_h = a + bm_\pi^2, \quad m_h = a + bm_\pi^2 + cm_\pi^4.$$

The difference between these two extrapolations gives some information on the systematic uncertainties in the extrapolated quantities. Although, our quark masses are quite small, both linear and quadratic fits essentially gave the identical results. The chiral uncertainties in the physical limit are significantly small (less than a percent) at our present statistics.

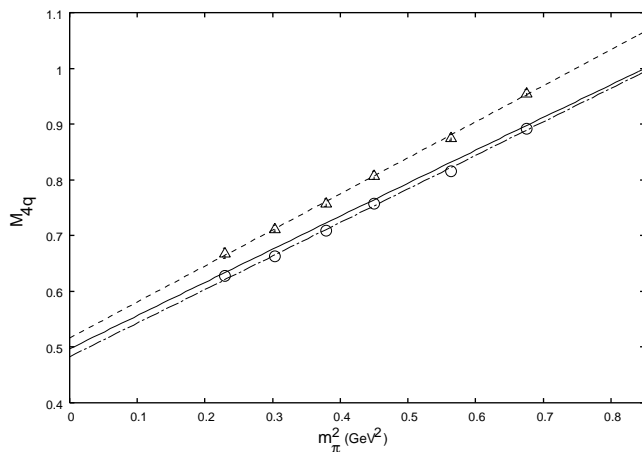


FIG. 4: Chiral extrapolation of effective masses in the $I = 0$ (open circles) and $I = 2$ (open triangles) channels. The solid curve denotes the two-pion threshold, and dashed curves are the linear fits to the data.

At smaller quark masses, the data for the $I = 0$ channel appear slightly below the two-pion threshold, by ~ 30 MeV, and seems to behave linearly in m_π^2 rather than the two-pion threshold which shows a quadratic behaviour in m_π^2 . The data for $I = 2$ lie above the two-pion threshold by $\sim 40 - 50$ MeV for all quark masses analysed here. If the slight difference from two-pion threshold can be explained by the two-pion interaction, then the lowest scalar $4q$ state can be regarded as a two-pion scattering state.

The results for the extracted mass for $J^P = 1^+$ are displayed in Fig. 5 as a function of m_π^2 . The ground-state masses for the tetraquark and two-particle states are again very different. The mass of the tetraquark state extracted is consistently higher than the lowest two-particle state, namely $\pi + \rho$. This trend continues in the physical limit where the masses exhibit the opposite behaviour to that which would be expected in the presence

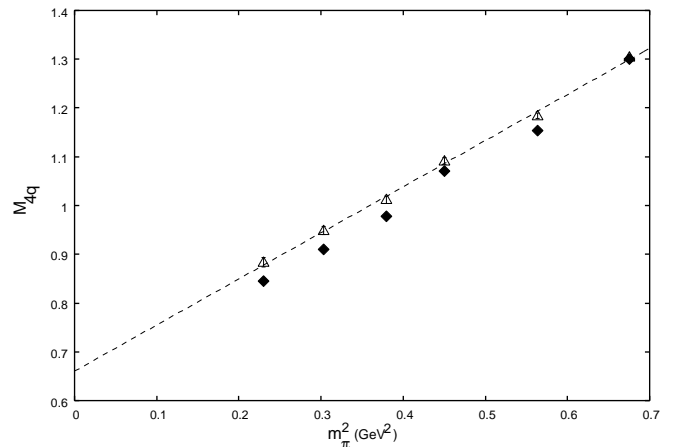


FIG. 5: Chiral extrapolation of effective masses in $I(J^P) = 1(1^+)$. The open triangles denote the $4q$ data and the solid diamonds denote the two-particle state ($\pi + \rho$). The dashed curve is a linear fit to the data.

of binding. In the chiral limit the $I = 1$ state lies above the two-pion threshold by ~ 70 MeV.

TABLE I: The masses of the $I(J^P) = 0(0^+), 2(0^+)$ and $I(J^P) = 1(1^+)$ $4q$ states in the lattice units for various values of κ_t .

κ_t	$J^P = 0^+$			$J^P = 1^+$
	M_ρ	$M_{4q}^{I=0}$	$M_{4q}^{I=2}$	$M_{4q}^{I=1}$
0.2610	0.850(2)	0.892(4)	0.956(6)	1.305(4)
0.2620	0.741(2)	0.815(5)	0.877(6)	1.174(6)
0.2635	0.687(3)	0.758(5)	0.808(7)	1.094(7)
0.2640	0.606(3)	0.709(6)	0.756(7)	1.012(7)
0.2650	0.572(3)	0.663(7)	0.712(6)	0.949(8)
0.2655	0.529(4)	0.627(8)	0.668(8)	0.884(9)

Since quenched spectroscopy is quite reliable for the mass ratio of stable particles, it is physically even more motivated to extrapolate the mass ratio instead of the mass. This allows for the cancellation of systematic errors since the hadron states are generated from the same gauge field configurations and hence systematic errors are strongly correlated. The mass ratios at hand show a remarkably small scaling violation; -hence, we adopt an m_π^2 -linear extrapolation for the continuum limit. We also perform an m_π -quadratic extrapolation to estimate systematic errors. Performing such extrapolations for all sets of masses, we adopt the choice which shows the smoothest scaling behaviour for the final value, and we use others to estimate the systematic errors.

The results of the mass difference analysis are shown in Table II and illustrated in Fig. 6. The data behave almost linearly in m_π^2 and both linear and quadratic fits essentially gave identical results. Again the contributions from the uncertainties due to chiral logarithms in the

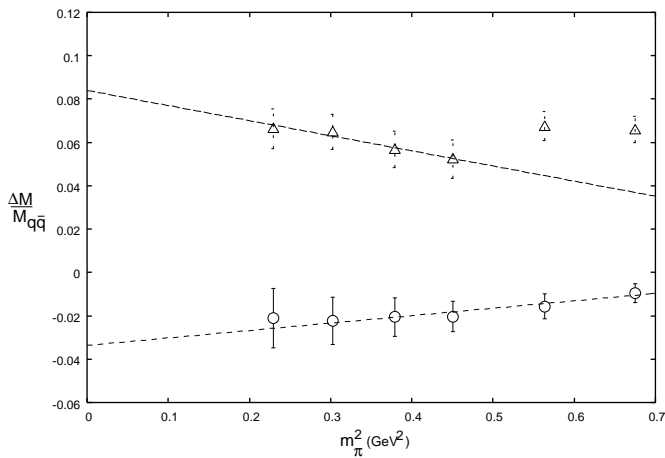


FIG. 6: Extrapolation of the mass ratios of the $I = 0$ (open circles) and $I = 2$ (open triangles) channels to the physical limit. The dashed lines are the linear fits in m_π^2 to the data.

physical limit are seen to be significantly less dominant.

The question whether the lowest-lying scalar $4q$ state extracted is a scattering state or a resonance is better resolved by analysing the ratio of the mass differences $\Delta M = M_{4q} - 2M_{q\bar{q}}$ (between the candidate lowest scalar $4Q$ state and the two-pion state) and the ρ mass.

The non-zero m_π^2 values of the ratio are within 0.01-0.02 standard deviations of the extrapolated zero pion mass result. This implies that the chiral uncertainties in the physical limit are less than 2%. The fitted results show that the mass difference ΔM and hence the mass ratio for the $I = 0$ channel are clearly negative and increase in magnitude as we approach the physical regime. This implies that the binding becomes stronger at light-quark masses with a general trend of negative binding as the zero quark mass limit is approached. In the physical limit, the negative mass difference is $\sim 25 - 30(2)$ MeV. Naively one may be tempted to interpret this negative mass splitting near the physical regime as a lattice resonance signature for scalar $4q$ resonance with $I = 0$. Using the chirally extrapolated value of the ratio $m_\pi/m_\rho = 0.60(1)$, the $I = 0$ state is found to have a mass of $m_{4q}^{I=0} = 927(12)$ MeV in the physical limit. The lowest scalar $4q$ state appears to be slightly lighter than the experimentally observed $f_0(980)$. It still remains to verify whether analysis at relatively large quark masses would affect the manifestation of the bound state and aid to confirm the indication of the resonance. This analysis is discussed in the next section. On the other hand the $I = 2$ channel again shows a positive splitting of the order of $\sim 50(4)$ MeV. This suggests that instead of a bound state, we appear to be seeing a scattering state in the $I = 2$ channel.

The behaviour observed for the mass differences between the $I = 1$ and the two-particle states is illustrated in Fig. 7. A positive mass splitting is observed for all the five smallest quark masses and increases as the phys-

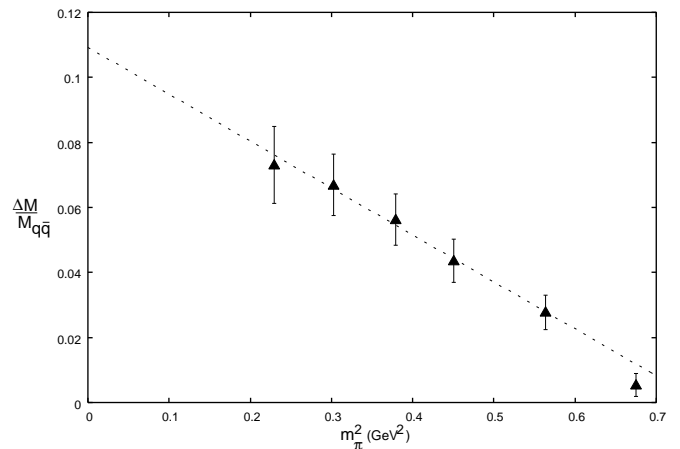


FIG. 7: As in Fig. 6, but for the $I(J^P) = 1(1^+)$ state.

ical regime is approached. The signature of repulsion at quark masses near the physical regime would imply no evidence of the resonance in the $I = 1$ channel. This suggests that the $I = 1$ tetraquark system (in the quenched approximation) is more complicated and different from the two-hadron system otherwise. Adopting a linear chiral extrapolation, the mass of the $I(J^P) = 1(1^+)$ tetraquark state is estimated as $M_{4q}^{J=1} = 1360(30)$ MeV which is lower than the mass of the experimentally observed $a_0(1474)$.

TABLE II: Ratios between the mass difference, ΔM_{4q} and m_ρ at various pion masses.

M_π (GeV)	$\Delta M_{4q}^{I=0}/M_\rho$	$\Delta M_{4q}^{I=2}/M_\rho$	$\Delta M_{4q}^{I=1}/M_\rho$
0.822	-0.0096(43)	0.0660(61)	0.0054(36)
0.751	-0.0016(54)	0.0674(67)	0.0278(53)
0.672	-0.0203(71)	0.0523(86)	0.0436(66)
0.616	-0.0206(88)	0.0568 (82)	0.0562(78)
0.550	-0.022(10)	0.0650(81)	0.0669(91)
0.479	-0.021(13)	0.0664(92)	0.0731(94)

As mentioned above, to obtain a definitive result for the signature of a possible scalar tetraquark bound state with $I = 0$ will require the implementation of the heavy quark limit. The heavy quark mass suppresses relativistic effects, which complicates the interpretation of light-quark states. By giving the quarks a larger mass would alter threshold, which in turn would affect the manifestation of the bound state. To confirm this, we calculate the mass of the lowest $4q$ state with varying quark mass. We allow the quark mass to be larger (hundreds of MeV) so that the continuum threshold for the decay $q^2\bar{q}^2 \rightarrow (q\bar{q})(q\bar{q})$ is elevated. The resulting extracted masses and mass differences are tabulated in Table III and shown in Fig. 8, respectively.

The ground-state masses in the scalar channel are slightly larger than those obtained at the small quark

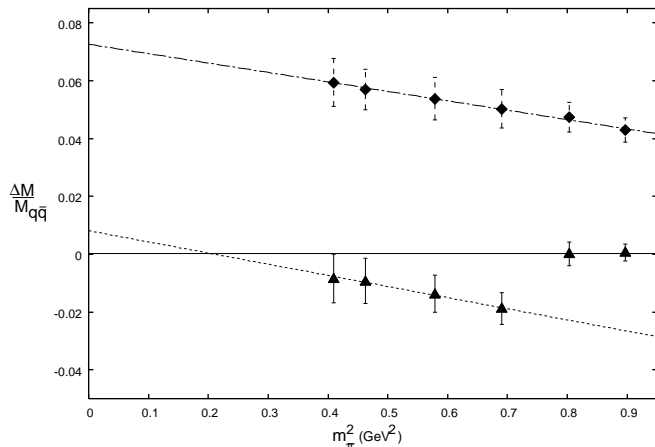


FIG. 8: Chiral extrapolation of the mass ratios at heavy quark masses. The solid triangles denote the $I = 0$, and solid diamonds represent the $I = 1$ tetraquark states, respectively. The dashed curves are linear fits to the data.

masses. The mass difference is consistent with or slightly below the mass of the lowest two-pion state at the four smallest quark masses. The mass difference appears to be approaching a positive constant near the physical limit and the tetraquark masses are ~ 50 MeV larger than the s -wave two-pion state. This suggests that instead of a bound state, we appear to be seeing a scattering state in the $I = 0$ channel. The lattice data for the $I = 1$ channel appear to be well above the increased two-particle state threshold and remains approximately constant with m_π^2 . In the chiral limit, the difference between the $I = 1$ $4q$ state and the two-pion threshold is ~ 80 MeV. Again, the positive mass difference could be a signature of repulsion in this channel. We conclude that there are no surprises in the $I = 1$ channel - no evidence of attraction and hence no indication of a resonance which could be interpreted as the $4q$ state.

TABLE III: Ratios between the mass difference, ΔM_{4q} and the m_ρ at large quark masses.

M_π (GeV)	$\Delta M_{4q}^{I=0}/M_\rho$	$\Delta M_{4q}^{I=1}/M_\rho$
0.947	0.0006(30)	0.0429(42)
0.896	0.0002(41)	0.0474(51)
0.830	-0.0188(55)	0.0503(67)
0.761	-0.0137(64)	0.0538(74)
0.680	-0.0093(78)	0.0570(70)
0.641	-0.0085(84)	0.0594(82)

Finally, we compute the potential V_{4q} as a function of the distance between the two diquark, R , and the internal diquark separation D . We calculate the ground-state potential from the behaviour of the Wilson loop, $\langle W_{4q} \rangle$, at large t for symmetric planar loops with $d_1 = d_2 = d_3 = d_4 = D$. The plateau for representative values of R and D are shown in Fig. 9. As a result of smearing

the plateaus are seen at earlier t , which indicates a good overlap with the state in question. The errors on all our data points are jackknife errors. In our analysis, we calculate the effective $4q$ potential by choosing a fit which has $\chi^2/\text{d.o.f} \lesssim 1$ and is insensitive to the fit parameters.

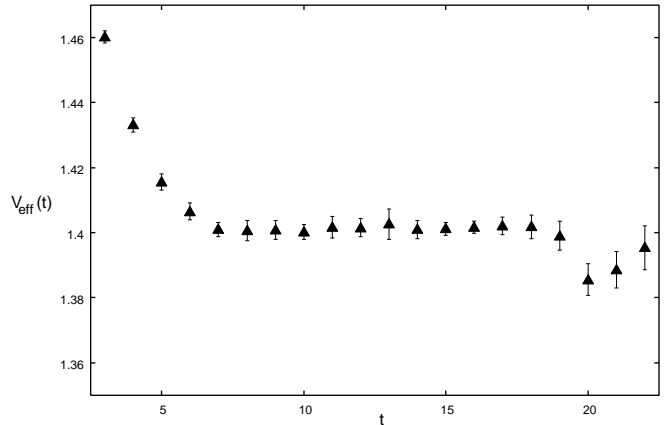


FIG. 9: Effective potential as a function of t in lattice units. The graph corresponds to the internal diquark separation $D = 2$ and diquark separation $R = 4$.

Fig. (10) shows the tetraquark potential as a function of the diquark separation R for different values of the internal diquark distance D . At small values of diquark separation and $R < D$, the data seem to coincide and the tetraquark potential converges to the two-meson Ansatz. Thus for these geometries the system corresponds to the two-meson state. For $R > D$ the tetraquark potential is lower than $2V_{q\bar{q}}(R)$ but seems to be in excellent agreement with one-gluon exchange Coulomb plus multi- Y Ansatz [23]. Comparing the V_{4q} and $2V_{q\bar{q}}$, we see that the tetraquark potential starts as a sum of the two-meson potential and then cross over to approach the connected $4q$ state. This would indicate that ground-state configuration is largely a tetraquark state for large R . The flip-flop between the $4q$ state into the two-meson state seems nontrivial.

Now all prerequisites are available to investigate the stability of the $4q$ state. We notice that when $q\bar{q}$ and $q\bar{q}$ are well separated, all the four quarks are linked by connected Y -shaped flux tube, where the total flux-tube length is minimised. This would mean that the examined $4q$ system can be qualitatively explained as a connected $4q$ state. On the other hand, when the nearest quark and antiquark are spatially close, the system is described as a two-pion state rather than a $4q$ system. Therefore, this type of flip-flop between the $4q$ and the two-pion state around the cross-over can be interpreted as a flux-tube recombination between the two mesons.

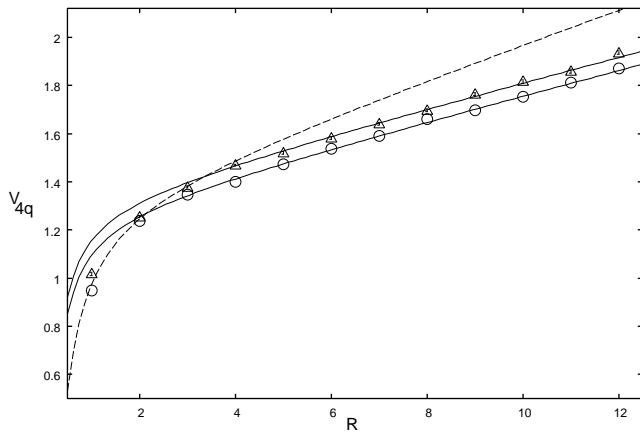


FIG. 10: Tetraquark potential V_{4q} for symmetric planar configurations at $D = 2$ (open circles) and $D = 4$ (open triangles), respectively. The solid curve represents the one-gluon exchange plus multi- Y Ansatz, and the dashed curve the two-meson Ansatz.

V. SUMMARY AND CONCLUSION

We have presented the results of our investigation of the tetraquark systems in improved anisotropic lattice QCD in the quenched approximation on relatively light- and heavy-quark masses. Our analysis takes into account all possible uncertainties, such as statistical uncertainties, finite size, and quenching errors when performing the chiral extrapolations. The masses of the $J = 0$ and $J = 1$ states were computed using field operators, which are motivated by the $\pi\pi$ and diquark structure. By analysing the correlation matrix we determined the masses of isospin 0, 1 and 2 channels. In the region of pion mass which we are able to access, we saw the evidence of attraction for the $I = 0$ channel. However, at relatively large quark masses, the manifestation of the bound state changes and $I = 0$ state appears to be the scattering state.

The observation of repulsion at both light- and heavy-quark masses is particularly evident in the $I = 1$ and $I = 2$ states. Both showed a positive splitting between tetraquark and two-pion states, suggesting repulsion as opposed to attraction. The evidence of repulsion could be associated with the absence of a resonance in both these channels. Moreover, in the case of $I(J^P) = 1(1^+)$ and $0(2^+)$, which are more exotic than the $0(0^+)$ state, the interpolators had sufficient overlap to allow for a successful correlation matrix analysis and produced no evidence of attraction that one might expect if a tetraquark state existed. This produces further evidence that there are no spatially-localised lowest-lying tetraquark states.

From our static tetraquark potential analysis we conclude that we showed that at small internal separation between diquarks and with internal diquark distance larger than the diquark separation ($R < D$), the tetraquark system is a two-meson state and its static potential is approximately given by the $2V_{q\bar{q}}$ potential. For $R > D$, the static potential is described by confining V_{4q} . In summary, these observations suggest that, the $4q$ system behaves as a multiquark state at diquark separation larger than the internal diquark distance. This behaviour is expected to hold for general diquark configurations. It will be essential to explore unquenched QCD to establish the existence or the absence of a tetraquark resonance in lattice QCD before one rules out the possible existence of a tetraquark state in full QCD.

Acknowledgments

We thank R. Jaffe and C. Michael for a number of valuable suggestions and useful comments on this work. We are grateful for the access to the computing facility at the Shenzhen University on 128 nodes of Deepsuper-21C. ML was supported in part by the Guangdong Provincial Ministry of Education.

-
- [1] LEPS Collaboration (T. Nakano *et al.*), Phys. Rev. Lett. **91**, 012002 (2003)
 - [2] DIANA Collaboration (V. Barmin *et al.*), Phys. Rev. Lett. **91**, 252001 (2003)
 - [3] CLAS Collaboration (V. Kubarovsky *et al.*), Phys. Rev. Lett. **92**, 032001 (2004)
 - [4] BES Collaboration (J. Bai *et al.*), Phys. Rev. **D70**, 012004 (2004)
 - [5] BES Collaboration, Phys. Lett. **B598**, 149 (2004)
 - [6] BES Collaboration, Phys. Lett. **B607**, 243 (2005)
 - [7] BES Collaboration (M. Ablikim, *et al.*), Phys. Lett. **B603**, 138 (2004)
 - [8] ZEUS Collaboration, Phys. Lett. **B578**, 33 (2004)
 - [9] Belle Collaboration (S. Choi *et al.*), Phys. Rev. Lett. **91**, 262001 (2003)
 - [10] CDFII Collaboration (D. Acosta *et al.*), Phys. Rev. Lett. **93**, 072001 (2004)
 - [11] BARBAR Collaboration (B. Aubert *et al.*), Phys. Rev. Lett. **93**, 041801 (2004); Phys. Rev. Lett. **90**, 242001 (2003)
 - [12] F. Close and S. Godfrey, Phys. Lett. **B574**, 210 (2003)
 - [13] F. Close and P. Page, Phys. Lett. **B578**, 119 (2004)
 - [14] S. Pakvasa and M. Suzuki, Phys. Lett. **B579**, 67 (2004)
 - [15] C. Wong, Phys. Rev. **C69**, 055202 (2004)
 - [16] E. Braaten and M. Kusunoki, Phys. Rev. **D69**, 074005 (2004)
 - [17] B. Lusscock *et al.*, Phys. Rev. **D72**, 014502 (2005) and references therein.
 - [18] F. Oikharu *et al.*, Phys. Rev. **D72**, 074503 (2005) and references therein.
 - [19] M. Fukugita *et al.*, Phys. Rev. **D52**, 3003 (1995)
 - [20] M. Alford and R. Jaffe, Nucl. Phys. B **578**, 367 (2000)

- [21] R. Gupta, A. Patel, and S. Sharpe, Phys. Rev. **D48**, 388 (1993)
- [22] S. Sharpe, R. Gupta, and G. Kilcup, Nucl. Phys. **B 383**, 309 (1992)
- [23] H. Suganuma, T. Takahashi, F. Oikharu, and H. Ichie, Nucl. Phys. **B** (Proc. Suppl.) **141**, 92 (2005)
- [24] C. Alexandrou and G. Koutsou, Phys. Rev. **D71**, 014504 (2005)
- [25] H. Suganuma, F. Oikharu, T. Takahashi, and H. Ichie, Nucl. Phys. **A755**, 399 (2005)
- [26] H. Suganuma, K. Tsumura, N. Ishii, and F. Oikharu, hep-lat/0707.3309v1
- [27] R. Jaffe and F. Wilczek, Phys. Rev. Lett. **91**, 232003 (2003)
- [28] C. Alexandrou and A. Tsapalis, Phys. Rev. **D73**, 014507 (2006)
- [29] T. Chiu and T. Hsieh, Phys. Rev. **D72**, 034505 (2005)
- [30] M. Albanese *et al.*, Phys. Lett. B **192**, 163 (1987)
- [31] C. Morningstar and M. Peardon, Phys. Rev. **D60**, 034509 (1999)
- [32] M. Okamoto, *et al.*, [CP-PACS Collaboration], Phys. Rev. **D65**, 094508 (2002)
- [33] P. Lacey *et al.*, [UKQCD Collaboration], Phys. Rev. **D51**, 6403 (1995)
- [34] N. Ishii *et al.*, Phys. Rev. **D71**, 034001 (2005)
- [35] D. Leinweber, A.W. Thomas, and R.D. Young, Phys. Rev. Lett. **92**, 242002 (2004)